NANO LETTERS

2001
Vol. 1, No. 11
617−623

Motion of Submicrometer Particles Dominated by Brownian Motion near Cell and Microfabricated Surfaces

Michelle S. Hale* and James G. Mitchell

Flinders University, School of Biological Sciences, P.O. Box 2100, Adelaide, SA, 5001, Australia

Received June 26, 2001; *Revised Manuscript Received August 14, 2001*

ABSTRACT

Control of submicrometer particles is essential for microfluidic devices. In microfluids, the current approach for achieving particle control relies on interaction between particles and patterned obstructions and requires complex manufacturing and purified samples. Here, we report how the rigid, silica frustules of diatoms, microscopic protists, control submicrometer particle movement on their open surfaces. This provides insight into how diatoms function in a particle-laden environment and suggests potentially useful open-channel principles and designs in microfluidics.

Recent advances in nanotechnology have shown the utility of open microchannels for controlling chemical reactions.[1−4] While considerable progress has been made for solutions, fluid-particle systems still present considerable technical challenges, particularly for biological samples where mixtures of complex molecules are common.[5] Particles in microfluidic systems continually encounter channel walls because of high surface area-to-volume ratios and the effectiveness of molecular diffusion over the characteristic micrometer distances. Unfortunately, particle surface interactions are poorly understood and can produce unpredictable or unexplainable results.[6] Previous experiments and models used flat surfaces and the controlling interactions were the short-range van der Waals force and longer-range electrostatic force.[7−9] In cell-fluid systems, ranging from blood to the ocean, high salt concentrations and membranes or other coatings reduce the Debye−Hückel length for electrostatic force to less than a few nanometers.[10] This leaves surface-induced drag on Brownian particles as the dominant process at suprananometer distances from surfaces.[11]

To better understand Brownian particle behavior in microfluidics and in cell surface biology, we examined how marine diatoms control particle distributions using their cell surface microtopographies. Diatoms are single-celled microalgae completely encased in porous, lattice-like silica frustules. These frustules exhibit surface structures ranging from molecular to microscopic, but their presence excludes cilia, flagella, and the uptake of large particles. The absence of these normal particle control processes, coupled with the geometric regularity of frustules, make diatoms ideal for examination and experimentation of microstructure-induced particle control by biological surfaces. Understanding such particle control may point to how microchannel walls might be textured to optimize chemical or biological reactions, while providing insight into diatom ecology.

Diatoms, unlike most biological surfaces, are solid and not membranaceous, and they present a single sharp focal plane under light and electron microscopy. Frustules of centric diatoms are covered with radial rows of hexagonal chambers, called areolae (Figure 1). Each chamber has an outer wall, exposed to the external environment, and an inner wall, close to the cell membrane. It is usual that one is perforated by a large round hole (foramen), while the other contains a porous plate, called a sieve plate.[12] The flux of nutrients and exudates across the cell membrane occurs at the base of each areola (the inner wall).[13] The species-specific size, arrangement, and structure of areolae have been well described for the 10,000−12,000 known species,[14] and morphology also varies within some species.[15]

Marine and freshwater diatoms are exposed to a range of living and nonliving Brownian particles. In the ocean, these include nutrient molecules ($\sim 10^{14}$ mL^{-1}), colloids (5 nm to 2 μm and $\sim 10^{7}-10^{9}$ mL^{-1} [16]), viruses (20−200 nm[17] and $\sim 10^{7}$ mL^{-1} [18]), and bacteria (0.2−1 μm and $\sim 10^{6}$ mL^{-1} [19]). Despite being continuously bathed in this array and concentration of particles, frustules are remarkably clean surfaces. The absence of flagella and cilia, combined with strong ionic screening by seawater, suggests that sorting, breakup, or dispersal of these particles occurs through drag interactions with the rigid, patterned surface microstructures.

* Corresponding author. E-mail: michelle.hale@flinders.edu.au. Phone: +61 8 8201 5234. Fax: +61 8 8201 3015.

10.1021/nl015575o CCC: $20.00
Published on Web 08/25/2001

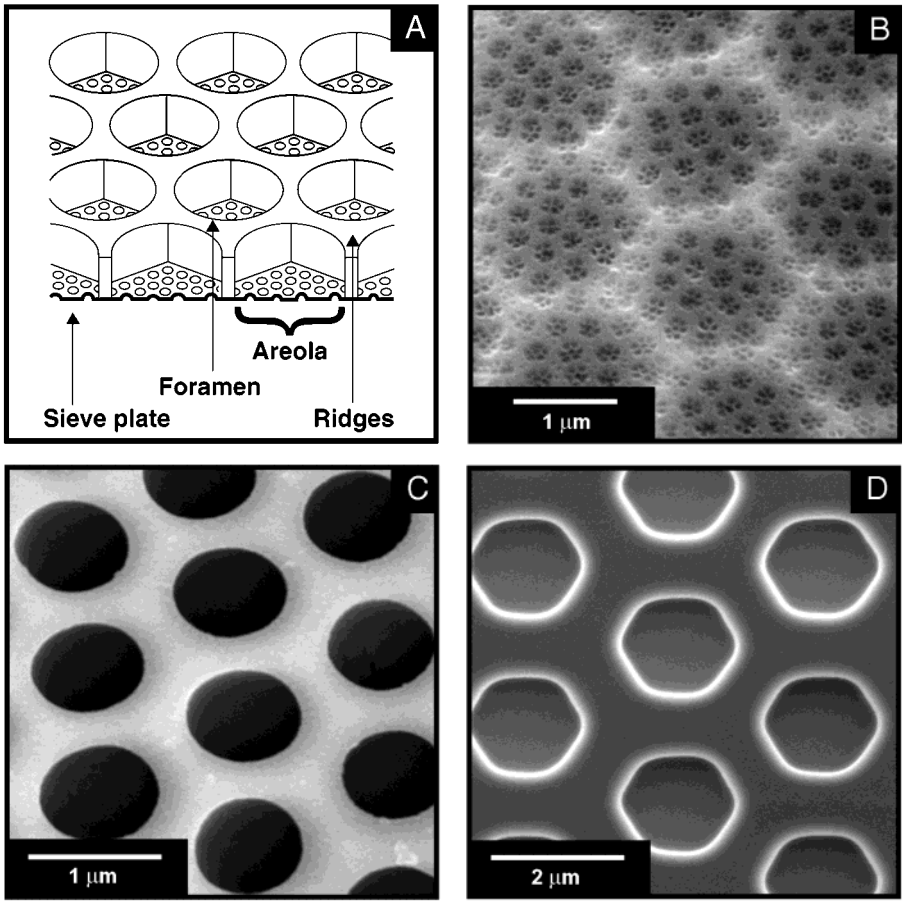

Figure 1. (A) Schematic representation of frustule structure of a centric diatom, showing the main features of areolae, including the hexagonal structure of each chamber and the presence of a porous sieve plate. The structure and arrangement of areolae within the frustules of centric diatoms are species-specific. Scanning electron micrographs (SEM) show the areolation patterns of cleaned centric diatom frustules of (B) *Coscinodiscus* sp., (C) *Thalassiosira eccentrica* and (D) the artificially constructed diatom mimic. In species such as *T. eccentrica*, areolae open to the external environment (outside) by foramen and open toward the cell membrane (inside) by a sieve plate. The structure of *Coscinodiscus* sp. areolae is reversed, with the foramen opening to the inside, and the frustule opening to the outside by a recessed sieve plate. The depth of each areola is approximately 1−2 μm.[12]

Here we show that the small-scale surface structures of diatom frustules alter the diffusion and advection of submicrometer particles, resulting in localized concentrations of particles on ridged areas surrounding areolae. This behavior was consistent with that of particles diffusing over an artificially constructed silicon diatom mimic. Variations in the hydrodynamic effects of surfaces on the diffusion and advection of Brownian particles may help explain the diverse range of frustule morphologies observed among diatoms, and demonstrate how passive surface microstructures may be used to control the diffusion of submicrometer particles near surfaces in integrated microfluidic devices.

To examine the effects of surface microtopographies on particle motion, live cells[20] of *Coscinodiscus* sp. and *Thalassiosira eccentrica* were attached to glass coverslips and placed in small flow chambers. The chamber design has been described elsewhere.[21] Live diatom cells were stuck on the underside of the coverslip with poly-lysine,[22] and movements of beads over the frustules of diatoms were recorded by video microscopy. To allow comparison between beads moving over frustules with beads moving over manufactured surface microstructures, beads were also recorded moving over artificially constructed hexagonal arrays (Figure 1D) and a glass coverslip. The diatom mimics were made at the Cornell Nanofabrication Facility, using standard photolithography techniques. The pores were etched into silicon, to a depth of 1 μm. Video microscopy allowed measurements of flow speeds 20 μm above the surface and the confirmation of laminar flow in the region of the chamber being examined. Artificial seawater solutions (35%, 20 °C, filtered through 0.24 μm) containing monodisperse, charge-stabilized, spherical fluorescent polystyrene (Molecular Probes) or latex (Sigma) beads with radii of 0.05, 0.1, 0.15, 0.25, 0.3, 0.4, 0.5, or 1 μm were used for experiments. NaCl, in solution, screened electrostatic interactions to approximately 4 nm, the Debye−Hückel screening length.[10] To ensure that interactions between beads were negligible,[23] the concentration of beads was such that the average separation distance was always larger than 16 μm.[6] We recorded the movement of beads over diatoms, the artificial diatom mimic, glass coverslips, and mid-chamber at flow rates of 0, 50, 100, and 800 μm s^{-1}, measured 20 μm above the surface. Flow decreases fractionally from the surface of a sphere by $1 - (1 - 3/4r - 1/4r^3)$, where r is the distance away from the surface (in units of sphere radii).[24] Therefore, for a cell with a radius of 50 μm, only 37% of the total shear occurs across

the first 20 μm distance from the cell surface. Thus, flow velocities of 50, 100, and 800 μm s^{-1}, measured at 20 μm away from the surface, correspond to far field velocities of 135, 270, and 2160 μm s^{-1}, respectively. Chambers were viewed under Nomarski optics and fluorescence video microscopy using a 100× oil immersion objective (numerical aperture = 1.3), with further magnification provided by 3.3 or 6.7 long distance coupling lenses to a Panasonic CCD camera (WV−BP550). Due to the depth of field of the objective, beads included in the analysis were no more than 1 μm from the surface and only beads observed to be in focus were used.

With no flow, deviations from unbiased Brownian motion were quantified by analyzing video footage of beads, frame by frame (1/25 s intervals), for 5.2 s. We measured the distance of beads from the center of the ridged areas surrounding each areola or hole and calculated the proportion of time beads spent on the ridged areas from 130 sequential frames of video footage, for each bead-surface combination. Experiments were replicated 5 times, each with a different diatom frustule or diatom mimic, to account for minor shape variation that occurs among frustules. To ensure that observed localizations of beads on ridged areas were due to the presence of the underlying microtopography, rather than an artifact of the surface area of ridged and unridged areas, control data were collected for beads diffusing over a flat glass surface. For controls, beads were followed frame-by-frame across a flat glass surface, with the 2-dimensional surface structure of each diatom species or the diatom mimic superimposed on the video screen. Independent sample *t*-tests were run in SPSS 8.0 to test for significant differences between the proportion of time that beads spent on the ridged areas of the diatoms compared to their controls.

The successive position of each bead was recorded for 1000 frames (20 s) for the 0.5, 1, and 2 μm beads and 100 frames (2 s) for the 0.1 and 0.2 μm beads, as the smaller bead sizes were difficult to resolve and rapidly disappeared from the focal plane. Video sequences were digitized to computer memory at 50 frames s^{-1} (IMAQ PCI-1408 monochrome image acquisition board, National Instruments, Austin, Texas). The resulting digital filmstrips were analyzed frame-by-frame for trajectories of movement by LabTrack (DiMedia, Kvistgaard, Denmark).[25] For each bead-surface combination, 10 bead paths were captured in each of 3 replicate chambers. The square of the displacement from each bead's original position was calculated, and the average square of the displacement (i.e., over 10 beads) was plotted as a function of time. The diffusion coefficient was calculated from the slope of the linear fit of the statistical average by dividing the slope by four.[26]

Under flow, deviations of bead movement from the direction of flow were determined using frame-by-frame analysis of video footage of beads moving across frustule surfaces and over flat glass slides. To ensure that location and orientation information from adjacent frames were statistically independent, we plotted autocorrelograms of the trajectory angle and found there were no significant auto-correlations between frames. The sequential positions of beads were also used to determine bead speed and the angle of deflection of beads from the direction of flow.

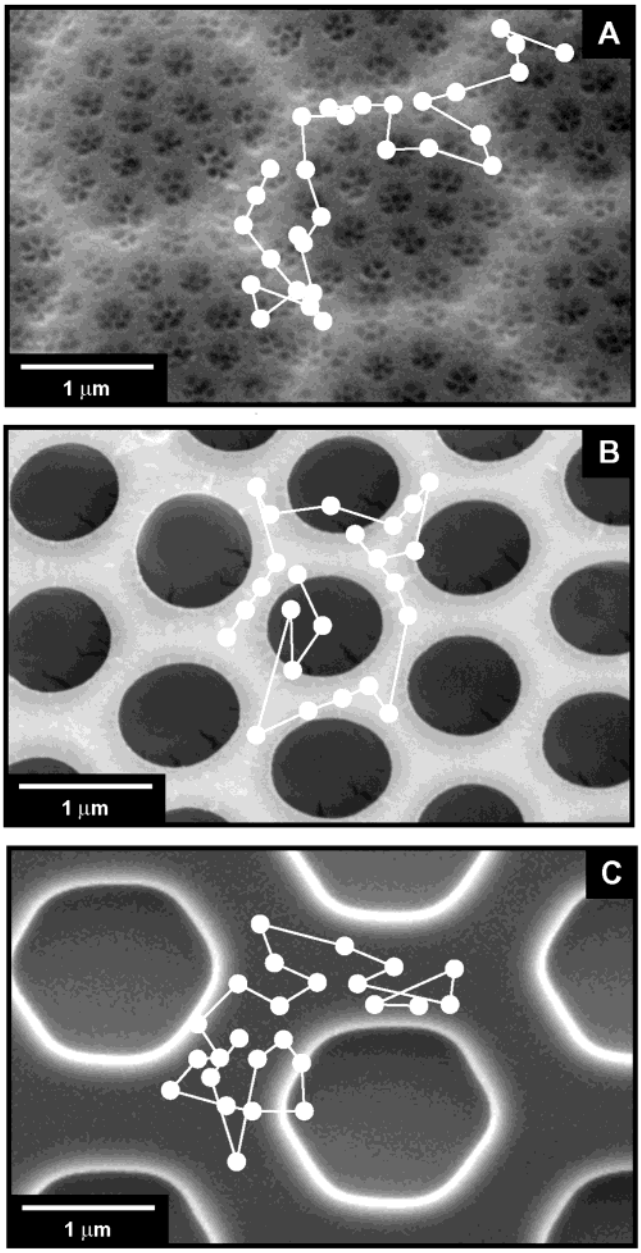

Figure 2. Diagrammatic representation of example paths of 0.25-μm radii beads diffusing over the surface of (A) *Coscinodiscus* sp., (B) *Thalassiosira eccentrica*, and (C) the artificially constructed diatom mimic. For each surface−bead combination, sequential frames of video footage (t = 0.04 s between frames) were viewed on a monitor and tracings were made of both the frustule surface and the bead path. Due to the regular nature of the areolation patterns of frustules and the diatom mimic, we were able to transcribe bead paths onto scanning electron micrographs of acid-washed surfaces, with circles representing the position of the center of each bead (± 0.06 μm), in sequential frames.

With no flow, localizations of beads on the ridged areas surrounding areolae were observed for *Coscinodiscus* sp., *T. eccentrica* and the diatom mimic. These localizations can be seen in the example bead paths in Figure 2. Figure 3A shows the significant differences ($p < 0.05$) in the proportion of time that 0.25-μm radii beads spent on the ridged areas

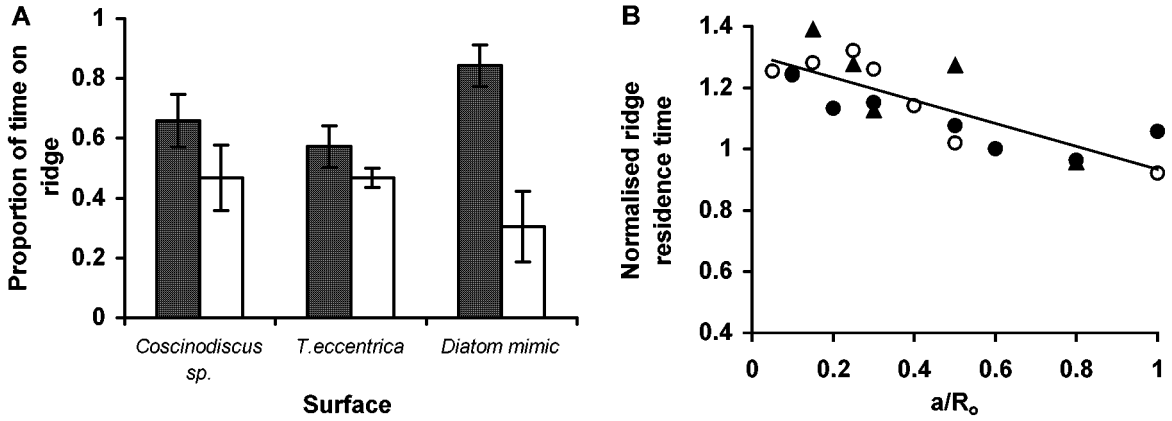

Figure 3. (A) Mean proportion of time 0.25-μm radii beads spent diffusing over live *Coscinodiscus* sp. and *Thalassiosira eccentrica* frustules and over the surface of the diatom mimic. All spent significantly higher proportion of time on ridges of the surfaces than their controls ($p < 0.05$). The error bars represent 95% confidence intervals ($n = 5$). (B) Normalized ridge residence time (NRRT) of beads over live *Coscinodiscus* sp. (○) and *T. eccentrica* (●) cells, and over the silicon diatom mimic (▲), as a function of the bead-to-areola radii (a/R_o). Normalized ridge residence time was calculated as the proportion of time beads spent on the ridges, divided by the ratio of the surface area of the ridges to the surface area of the areolae. Equation of the fitted trendline is NRRT $= -0.4\ (a/R_o) + 1.3$ ($r^2 = 0.66$, $p < 0.001$).

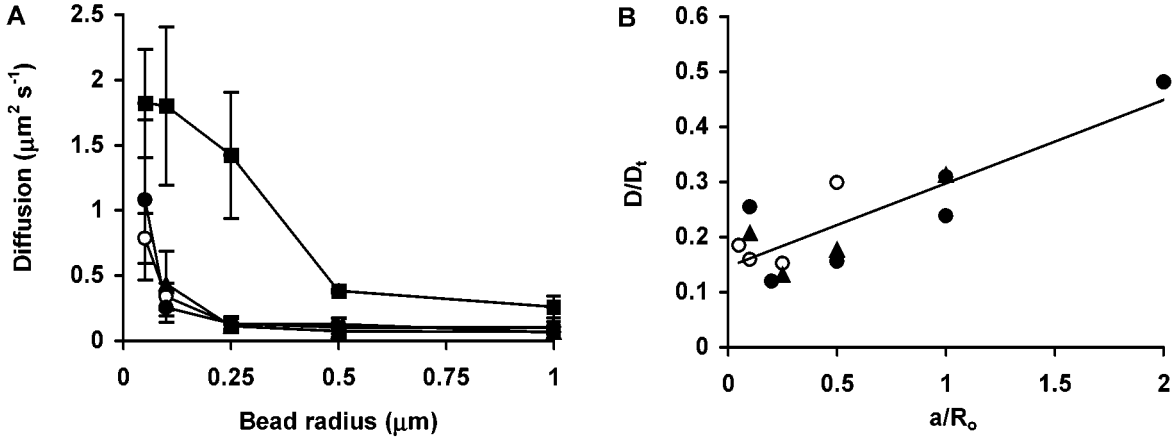

Figure 4. (A) Diffusion coefficients of beads moving over the frustules of live *Coscinodiscus* sp. (○), *T. eccentrica* (●), the diatom mimic (▲), and a glass slide (■). Beads with radii 0.1−0.5 μm diffused significantly slower over the frustules of the diatoms and the diatom mimic, compared to those diffusing over glass and mid-chamber ($p < 0.01$). Error bars are standard deviations ($n = 3$). (B) The effect of areolae on relative bead diffusion (D/D_t), as a function of the ratio of bead-to-areola radii (a/R_o), where D is the experimentally determined diffusion and D_t is the theoretical diffusion coefficient for beads diffusing in an unbounded medium. Equation of the fitted trendline is $D/D_t = 0.15\ (a/R_o) + 0.15$ ($r^2 = 0.71$, $p < 0.001$).

of each surface, compared to the controls. For particles diffusing across the surface of diatom frustules or the diatom mimic, this meant along-ridge movement was more likely than cross-ridge movement, maintaining and hence localizing beads on the ridged structures of surfaces. In addition, the mean proportion of time that 0.25-μm beads spent over the ridged areas of the diatom mimic was 1.3 times higher than over *Coscinodiscus* sp. ($p = 0.07$), and 1.5 times higher than over *T. eccentrica* ($p = 0.009$). The range of bead sizes that was significantly affected by the presence of underlying surface microstructures was different for the three surfaces. Beads with radii 0.05−0.5 μm were significantly localized on the ridged areas of *Coscinodiscus* sp. For *T. eccentrica* and the diatom mimic, the range was 0.15−0.5 μm.

Localizations of beads on the ridged areas surrounding diatom areolae and holes in the diatom mimic were due to variations in the drag experienced by beads as they diffused across the surfaces. Dagan et al.[27] have shown that for a sphere diffusing across a flat surface toward a single circular pore, with a sphere-to-pore ratio of less than one, drag is greatest when the sphere is on the solid part of the surface. Drag then decreases as the sphere moves to the edge of the pore, with a minimum value at the center of the pore opening. For spheres diffusing parallel to the surface, the effect is most significant close to the opening of the pore and when spheres are less than five sphere diameters away, perpendicular to the surface.[27] For diatom frustules and the artificial hexagonal array, this means that diffusion of beads is slower over ridged areas than over areolae, resulting in beads spending proportionally more time diffusing over ridges and resulting in localized concentrations on ridges. For diatoms and artificially constructed diatom mimics, this effect would be most significant for species with foramen opening to the outside (e.g., *T. eccentrica*), but was also seen in *Coscinodiscus* sp., as the sieve plate covering the cell surface was thin, porous, and recessed into each areola. Frustules are

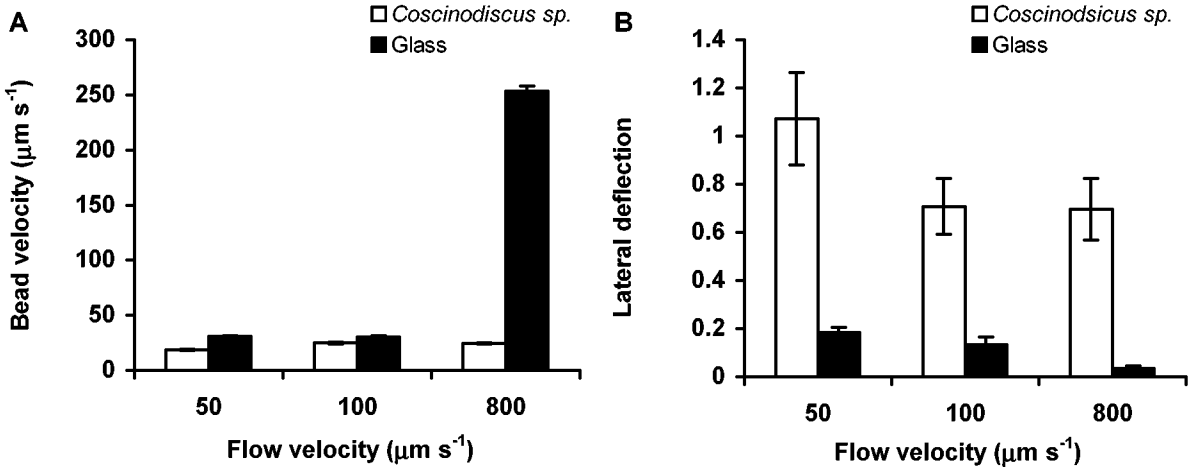

Figure 5. (A) Velocity of beads with 0.25 μm radii, flowing across the frustule of live *Coscinodiscus* sp. and over a flat glass surface, measured from video footage. Error bars are 95% CI ($n = 250$ for flow velocities of 50 and 100 μm s^{-1}, $n = 70$ for 800 μm s^{-1}, measured 20 μm above the surface). (B) Lateral deflection of bead trajectories from the direction of flow, for 0.25 μm radii beads flowing across the frustule of live *Coscinodiscus* sp. and over a flat glass surface. Lateral deflection was calculated as the distance that a bead travelled perpendicular to the flow, divided by the distance it travelled in the direction of flow, between sequential frames of video footage. A value of 1 indicates where a bead moved 1 unit distance horizontally to the flow, for every 1 unit distance it moved with the flow.

covered with regular arrays of closely spaced areolae, therefore the drag experienced by beads varies consistently across the entire surface and may alter the diffusion of Brownian particles up to 5 μm above the frustule.[27] This distance is much larger than 4 nm, the maximum distance that electrostatic force operates. The localization effect would also be strongest for flat ridges, where the drag experienced by a particle would be maximized. As the ridged areas of *T. eccentrica* appear to curve slightly toward the opening of the areolae, compared to the relatively flat surface of the diatom mimic, this may explain the significantly higher localization of beads observed over the diatom mimic.

Models developed by Miyazaki and Hasimoto[7] and Yan et al.[28] have examined the creeping motion of a small sphere with radius, a, toward a circular pore with radius, R_o, on a flat plate and predict that the effect on particle diffusion is greatest when a/R_o is small (0.1). Thus, the ratio of the sphere-to-pore radii (a/R_o) determines the extent of the effects of pores on diffusing spheres, rather than the radius of the sphere or pore exclusively.[7,28] Our data are in agreement with modeled predictions, as small values of a/R_o resulted in beads spending a higher proportion of time diffusing over the ridged areas, for both diatom species and for the artificial hexagonal array (Figure 3B). Data were normalized to account for differences in the ratio of the surface areas of the ridged (SA_r) to nonridged (SA_a) surfaces. Data were normalized by dividing the proportion of time that beads spent on the ridges by SA_r/SA_a, resulting in a normalized ridge residence time (NRRT) and allowing comparisons to be made between surfaces. A significant linear relationship ($p < 0.001$) was observed between NRRT and a/R_o, given by the equation $\text{NRRT} = -0.4(a/R_o) + 0.7$ (Figure 3B).

The localizations of beads on the ridged areas, described above, were due to increased drag experienced by the beads as they diffused across ridged areas of the frustule surface or the artificial hexagonal array. Experimentally determined diffusion coefficients of beads with radii of 0.1−0.5 μm diffusing over diatom frustules and over the diatom mimic, were also significantly lower than for beads diffusing over flat glass surfaces ($p < 0.001$) (Figure 4A). Reductions in bead diffusion showed a linear relationship with a/R_o (Figure 4B). Just as small values of a/R_o increased the proportion of time beads spent on the ridged areas, they also had the greatest effect on the reduction of diffusion. Our results show that the foramen-ridge complex of frustules causes size-specific drag maxima, suggesting that the different foramen-ridge complexes of diatom species have distinct effects on particles. Differential drag across the frustule of an individual diatom would result in the sorting of particles at the frustule surface and may operate to sort smaller particles at the porous sieve plate within the frustule. If sorting occurs at the sieve plate as well as at the ridge-areolar surface, as seems consistent with theory and our observations, then particle processing must be considered one of the primary functions of diatom frustules.

As well as affecting diffusion of particles close to the surface, the presence of areolae may also affect osmotic flux of particles by altering concentration gradients close to surfaces. Results of a model developed by Yan et al.[29] predicted that osmotic flux through a large, shallow pore may be overestimated by up to 200% for small particles ($a/R_o = 0.01$), if effects of pores are not considered. Although we were unable to resolve particles with radii smaller than 0.05 μm ($a/R_o = 0.05-0.1$), the model of Yan et al.[29] predicts that effects of areolae on osmotic flux would be greatest for particles with radii <10 nm, the size range that includes potential nutrients. Changes in the diffusion and osmotic flux of particles due to frustule microstructures may have important implications for both particle sorting and nutrient uptake by diatoms, by determining the material that reaches the cell wall and by altering the rate of nutrient flux through the frustule to the cell membrane. This mechanism may also

have useful applications for particle sorting and sieving in microfluidic devices.

The results described above show that diatom surfaces are capable of altering the diffusion of particles in a stagnant environment. However, diatoms exist in an environment of continuous flow and indeed depend on flow to replenish nutrients in the surrounding water. Similarly, microchannel walls are exposed to flow. Therefore, for the above results to be meaningful in diatom ecology or useful in microengineering applications, it is important to determine whether the effects of diatom surface microstructures on particle motion are maintained in the presence of flow.

At the low Reynolds numbers of diatom frustules and microchannels, when a particle approaches a flat surface, hydrodynamic interactions between the particle and the surface increase the viscous drag experienced by the particle.[30−31] The Reynolds number, $\mathrm{Re} = lU/\upsilon$, is a dimensionless ratio of the inertial to viscous forces that depend on length (l), velocity of the fluid (U), and the kinematic viscosity (υ). The Re permits comparisons of the dynamics of different systems. Laminar flow occurs in systems with low Re ($< \sim 1$), and systems with high Re ($> \sim 500$) are characterized by turbulent flow.

The hydrodynamic resistance experienced by the particle can differ substantially from the Stokes resistance of a particle in an unbounded fluid,[28] creating a region of shear between the wall and the fluid above. For phytoplankton, shear flow is already known to be important in determining near-surface nutrient dynamics[32,33] and the aggregation and disaggregation of colloids,[34−35] but there is no research on the mechanism. We found that the presence of areolation patterns on diatom frustules in flowing seawater further reduced particle velocities from those over flat glass surfaces. Bead velocities were up to an order of magnitude slower over diatom surfaces than over flat glass (Figure 5A). In addition to reduced velocities, beads experienced lateral deflection away from the direction of flow. We defined lateral deflection as the displacement of the bead perpendicular to the direction of flow divided by the displacement of the bead in the direction of flow. Beads deviated more than 1 unit distance perpendicular to the direction of flow, for every unit distance moved in the direction of flow (Figure 5B), with lateral deflection being greatest at the lowest flow velocity tested (50 μm s^{-1}).

Under flow conditions, frustule microstructures altered the behavior of particles at the surface, including those in the size range for colloids. The hydrodynamic effects of areolae on shear flow across the frustule can explain the deviation of particles from the direction of flow. Models developed to examine shear flow over pores of different shapes, radii, and depths have shown that pore morphology is important in determining the streamlines of flow.[36] For a shallow cylindrical pore at low Reynolds number, similar to the areolae of diatoms used in this study, streamlines follow the rim of the pore as water moves over the surface. This effect is limited to the region at the rim of the pore, where shear stresses change rapidly. At the downstream edge of the rim, shear stresses resume to the unperturbed values corresponding to simple shear flow over a flat surface.[36] As frustule surfaces are covered with regular arrays of closely spaced areolae, it is likely that shear flows remain perturbed over the entire surface. For diatom frustules, this means that beads following streamlines are directed around the edge of areolae and remain on the ridged areas of the frustule, resulting in deflections of beads from the direction of bulk flow. This behavior was observed in video footage, where beads were seen to move along the ridged parts of the surface. Although other forces, such as shear-induced lift,[37] may act to transport particles vertically away from the surface, the limited depth of field used in this study meant that any beads affected by these forces were not included in the analysis.

The principles learned from examining flow over frustule microstructures may prove useful in some areas of microfluidics, including fabrication using laminar flow (FLO).[38] FLO can generate a variety of microstructures, which are created when chemical reactions occur between multiple liquid streams flowing laminarly;[38] however, the structures that can be generated are currently limited by the types of laminar flow patterns available.

Diatom frustules and an artificially manufactured diatom mimic altered both the diffusion and advection of microscopic and submicroscopic particles. This may act as a particle sorting mechanism for diatoms, determining which material reaches the cell membrane and its receptors. As such, frustule surface structures and their effects on diffusive and advective processes may be crucial in understanding cell growth dynamics and may help explain the diversity of frustule structures observed among diatoms. Furthermore, the ability of diatom frustules to passively control the diffusion and advection of particles, the diversity of frustules that exists, and the ability to culture them in the laboratory makes their study potentially useful in the manufacture of a variety of nanotechnological devices.

Acknowledgment. We thank J. R. Seymour for laboratory assistance and P. Jumars, R. L. Waters, and two anonymous reviewers for their comments on the manuscript. G. Baxter, G. Bordonaro, M. Skvarla, and other staff of the Cornell Nanofabrication Facility provided training and direction in chip production. This work was funded by the Australian Research Council, Flinders University, and the U.S. National Science Foundation.

References

(1) Duke, T. A. J.; Austin, R. H. *Phys. Rev. Lett.* **1998**, *80*, 1552−1555.
(2) Chou, C.; Bakajin, O.; Turner, S. W. P.; Duke, T. A. J.; Chan, S. S.; Cox, E. C.; Craighead, H. G.; Austin, R. H. *Proc. Natl. Acad. Sci. U.S.A.* **1999**, *96*, 13762−13765.
(3) Kenis, P. J. A.; Ismagilov, R. F.; Whitesides, G. M. *Science* **1999**, *285*, 83−85.
(4) Chou, C.; Austin, R. H.; Bakajin, O.; Tegenfeldt, J. O.; Castelino, J. A.; Chan, S. S.; Cox, E. C.; Graighead, H.; Darnton, N.; Duke, T.; Han, J.; Turner, S. *Electrophoresis* **2000**, *21*, 81−90.
(5) Weigl, B. H.; Yager, P. *Science* **1999**, *283*, 346−347.
(6) Feitosa, M. I. M.; Mesquita, O. N. *Phys. Rev. A* **1991**, *44*, 6677−6685.
(7) Miyazaki, T.; Hasimoto, H. *J. Fluid Mech.* **1984**, *145*, 201−221.
(8) Song, L.; Elimelech, M. *J. Colloid Interface Sci.* **1995**, *173*, 165−180.
(9) Faibish, R. S.; Elimelech, M.; Cohen, Y. *J. Colloid Interface Sci.* **1998**, *204*, 77−86.

(10) Kaplan, P. D.; Faucheux, L. P.; Libchaber, A. J. *Phys. Rev. Lett*. **1994**, *73*, 2793−2796.
(11) Kao, M. H.; Yodh, A. G.; Pine, D. J. *Phys. Rev. Lett*. **1993**, *70*, 242−245.
(12) van der Hoek, C.; Mann, D. G.; Jahns, H. M. *Algae: An Introduction to Phycology*; Cambridge University Press: Cambridge, 1995.
(13) Round, F. E.; Crawford, R. M.; Mann, D. G. *The Diatoms, Biology and Morphology of the Genera*; Cambridge University Press: Cambridge, 1990.
(14) Hasle, G. R.; Syvertsen, E. E. *Identifying Marine Diatoms and Dinoflagellates*; Tomas, K., Ed.; Academic Press: San Diego, 1996; pp 5−386.
(15) Babanazarova, O. V.; Likhoshway, Y. V.; Sherbakov, D. Y. *Phycol*. **1996**, *35*, 113−123.
(16) Wells, M. L.; Goldberg, E. D. *Limnol. Oceanogr*. **1994**, *39*, 286−302.
(17) Ackerman, H. W.; Dubow, M. S. *Viruses of Prokaryotes*; CRC Press: Boca Raton, 1987.
(18) Hennes, K. P.; Suttle, C. A. *Limnol. Oceanogr*. **1995**, *40*, 1050−1055.
(19) Ducklow, H. W.; Shibah, F. *Aquatic Microbiology: An Ecological Approach*; Ford, T. E., Ed.; Blackwell Scientific Publications: London, 1993; pp 261−287.
(20) Hasle, G. R.; Fryxell, G. A. *Trans. Am. Microsc. Soc*. **1970**, *89*, 469−475.
(21) Hale, M. S.; Mitchell, J. G. *Aquat. Micro. Ecol.* **2001**, *24*, 287−295.
(22) Marchant, H. J.; Thomas, D. P. *J. Micro.* **1983**, *131*, 127−129.
(23) Crocker, J. C. *J. Chem. Phys*. **1997**, *106*, 2837−2840.
(24) Batchelor, G. K. *An Introduction to Fluid Dynamics*; Cambridge University Press: Cambridge, 1967.
(25) Blackburn, N.; Fenchel, T.; Mitchell, J. *Science* **1998**, *282*, 2254−2256.
(26) Faucheux, L. P.; Libchaber, A. J. *Phys. Rev. E* **1994**, *49*, 5158−5163.
(27) Dagan, Z.; Weinbaum, S.; Pfeffer, R. *J. Fluid Mech.* **1982**, *117*, 143−170.
(28) Yan, Z.; Weinbaum, S.; Ganatos, P.; Pfeffer, R. *J. Fluid Mech*. **1987**, *174*, 39−68.
(29) Yan, Z.; Weinbaum, S.; Pfeffer, R. *J. Fluid Mech*. **1986**, *162*, 415−438.
(30) Brenner, H. *Chem. Eng. Sci*. **1961**, *16*, 242−1564.
(31) Walz, J. Y.; Suresh, L. *J. Chem. Phys*. **1995**, *103*, 10714−10725.
(32) Karp-Boss, L.; Boss, E.; Jumars, P. *Oceanogr. Mar. Biol. Annu. Rev*. **1996**, *34*, 71−107.
(33) Pahlow, M.; Riebesell, U.; Wolf-Gladrow, D. A. *Limnol. Oceanogr*. **1997**, *42*, 1660−1672.
(34) Chin, W.; Orellana, M. V.; Verdunga, P. *Nature* **1998**, *391*, 568−572.
(35) Serra, T.; Casamitjana, X. *J. Colloid Interface Sci*. **1998**, *206*, 505−511.
(36) Pozrikidis, C. *Phys. Fluids* **1994**, *6*, 68−79.
(37) Belfort, G.; Davis, R. H.; Zydney, A. L. *J. Membr. Sci.* **1994**, *96*, 1−58.
(38) Burns, M. A.; Johnson, B. N.; Brahmasandra, S. N.; Handique, K.; Webster, J. R., Krishnan, M.; Sammarco, T. S.; Man, P. M.; Jones, D.; Heldsinger, D.; Mastangelo, C. H.; Burke, D. T. *Science* **1998**, *282*, 484−487.

NL015575O